Optimizing Excess-Oxygen Control in an Industrial Walking-Beam Reheating Furnace: A Replicated 2^3 Factorial Study of Scale Loss, Fuel Use, and Emissions Trade-offs

Gan Yimyam[1] Peerakarn Banjerdkij[2] and Ailada Treerattrakoon[3]

[1, 2] Department of Environmental Engineering, Faculty of Engineering, Kasetsart University, Bangkok, Thailand

[3] Department of Industrial Engineering, Faculty of Engineering, Kasetsart University, Bangkok, Thailand

Corresponding author: Peerakarn Banjerdkij

ABSTRACT

Background: Reheating furnaces in hot-rolling steel mills are simultaneously energy-intensive and yield-critical assets, accounting for 15–20% of total plant energy consumption while directly governing metallic yield through furnace-atmosphere-dependent oxidation kinetics. Excess oxygen accelerates iron-oxide scale formation and reduces saleable output, but oxygen minimization must be balanced against combustion stability, specific fuel consumption, and regulated emissions—a multi-objective trade-off that remains poorly characterized at industrial scale under real production disturbances.

Methods: This study reports a replicated 2^3 full factorial industrial experiment conducted in a natural-gas-fired walking-beam reheating furnace (24 m × 13 m × 5 m, three combustion zones) in Thailand. Three controllable operational factors were evaluated at two levels each: (X1) air–fuel control strategy (uniform excess air, $\lambda = 1.10$ across all zones, versus zone-differentiated lambda staging with $\lambda = 0.90/1.00/1.10$ in soaking/heating/preheating), (X2) furnace pressure setpoint (10 Pa vs. 20 Pa), and (X3) discharge-door state (closed vs. open). Sixteen fully randomized runs (two replicates per treatment) were conducted. The primary response was dry flue-gas O_2 (%); secondary responses included specific scale loss (kg/t steel), metallic yield (%), specific natural-gas consumption (Nm^3/t), and CO/NOx concentrations (ppm). A process-boundary carbon-economic screening translated results to kg CO_2e/t steel and USD/t steel.

Results: Dry flue-gas O_2 ranged from 3.84% to 13.17% across the factorial space. The fitted model achieved $R^2 = 0.986$ (adjusted $R^2 = 0.974$). Air–fuel strategy was the dominant main effect (+4.53 %-points, $p < 0.001$), followed by door state (+2.81 %-points, $p < 0.001$). The furnace pressure × door-state interaction was strongly significant (−1.40 %-points, $p < 0.001$), demonstrating that higher pressure suppresses infiltration-driven O_2 excursions only during door-open events. The recommended regime (lambda staging + door-state-conditional pressure) reduced mean O_2 from 7.04% to 3.90%, lowered scale loss by 17.7% (21.64 → 17.82 kg/t steel), and raised metallic yield from 97.83% to 98.21%. Specific natural-gas consumption increased 11.4% (48.29 → 53.81 Nm^3/t) and CO rose to 22 ppm, while NOx remained stable at 12–14 ppm. The net process-boundary carbon change was +2.85 kg CO_2e/t steel (+0.20 USD/t at 70 USD/tCO_2e); combined operational value from yield recovery and reduced scale handling yielded a net economic gain of +0.94 USD/t steel.

Conclusions: Excess-oxygen control in industrial walking-beam furnaces is fundamentally a coupled stoichiometry–infiltration problem. The interaction between furnace pressure and door

state is the key mechanism, requiring a door-state-conditional pressure strategy rather than a fixed setpoint. The recommended regime delivers statistically grounded, implementable, and economically positive material-efficiency improvements in existing fuel-fired reheating assets, with transparent quantification of energy and carbon trade-offs.

Keywords: walking-beam reheating furnace; excess oxygen; staged combustion; lambda staging; air infiltration; oxidation scale loss; full factorial design; design of experiments; material efficiency; decarbonization; carbon-economic trade-off; steel industry

1. Introduction

Steel production is among the most energy-intensive and carbon-intensive manufacturing activities globally, responsible for approximately 7–9% of direct fossil-fuel CO_2 emissions (International Energy Agency [IEA], 2023). Within integrated and semi-integrated mills, reheating furnaces occupy a dual role as energy consumers and yield governors: they condition billets, blooms, or slabs to rolling temperature (typically 1,150–1,280 °C) while the furnace atmosphere simultaneously dictates the rate of iron-oxide scale formation on the steel surface. The World Steel Association (2025) reported a sector-average greenhouse-gas intensity of 2.18 tCO_2e per tonne of crude steel and a material efficiency of 92.79% for 2024, underscoring that avoidable yield losses and process by-products remain systemically significant. Recent comprehensive reviews confirm that iron and steel rank among the hardest sectors to decarbonize owing to process constraints, capital lock-in, and the limited commercial readiness of breakthrough technologies such as hydrogen-based direct reduction (Kim et al., 2022; Kim et al., 2024), which amplifies the value of near-term operational improvements in existing assets.

Oxidation scale is a multi-layer iron-oxide product (wüstite, FeO; magnetite, Fe_3O_4; hematite, Fe_2O_3) that forms on the steel surface during high-temperature reheating. The rate of scale formation is governed by solid-state diffusion through the oxide layers and is a strong function of temperature, time at temperature, and, critically, the partial pressure of oxidizing species (primarily O_2 and H_2O) in the furnace atmosphere (Kofstad, 1988). Scale losses in industrial walking-beam furnaces typically range from 0.5% to 2.5% of charged mass, representing a direct reduction in saleable output, a solid-waste stream requiring collection and disposal, and a secondary quality concern if residual scale embeds into the rolled product surface. Recent semi-industrial experiments confirm that scale formation rate and morphology are highly sensitive to atmosphere composition, including O_2 content and the relative proportion of combustion products (Schwarz et al., 2025; Xu et al., 2024). Consequently, lowering excess oxygen is a technologically straightforward lever for improving material efficiency—but one that must be balanced against combustion stability, fuel consumption, and emissions constraints.

Excess oxygen in combustion flue gas is conventionally controlled by adjusting the air-to-fuel lambda ratio (λ). However, industrial walking-beam furnaces deviate substantially from laboratory idealization. Air infiltration through the charging/discharge aperture, furnace door gaps, and structural imperfections can dominate flue-gas O_2 independently of—and sometimes overwhelmingly above—the burner stoichiometry setting (Trinks et al., 2004). Furnace internal

pressure is the primary engineering control for infiltration: a slightly positive gauge pressure (5–25 Pa) creates an outward pressure gradient that resists inward ambient-air flow. The effectiveness of pressure control depends non-linearly on aperture geometry and door state, creating an interaction structure that has rarely been characterized experimentally at full industrial scale.

Recent studies has substantially advanced mechanistic understanding through full-scale combustion and heat-transfer modelling (Gan et al., 2024), oxygen-enrichment analysis (Khalid et al., 2021; Zhao et al., 2025), energy-saving studies coupling structural and combustion optimization (Lu et al., 2025), semi-industrial scale formation experiments under hydrogen and oxy-fuel conditions (Schwarz et al., 2025), and oxidation modelling under mixed-loading scenarios (Xu et al., 2024). Staged-air combustion has been shown to suppress thermal-NOx in reheating applications when zone-level oxygen is carefully managed (Sung et al., 2021). Despite these advances, a critical gap persists: no full-scale factorial study has simultaneously quantified the main and interaction effects of stoichiometry strategy, furnace pressure setpoint, and door-state-driven infiltration on excess oxygen and the downstream trade-off surface (scale loss, yield, fuel use, CO, NOx) under real production conditions. This gap matters because industrial process-heat decarbonization is an inherently multi-objective decision problem requiring robust operating rules under production variability, not single-point optima derived from idealized conditions (McMillan & Wachs, 2024).

This study addresses the identified gap by conducting a replicated 2^3 full factorial industrial experiment in a natural-gas-fired walking-beam reheating furnace in Thailand. It offers three specific and novel contributions: first, it provides factorial experimental evidence at a full industrial scale under real production constraints, highlighting the magnitude and statistical significance of the main and interaction effects of air–fuel strategy, furnace pressure setpoint, and discharge-door state on dry flue-gas O_2. Second, it introduces a door-state-conditional pressure control rule that directly links lambda staging to dynamic pressure management, which can be implemented in existing Level II combustion-control systems without hardware modification. Third, it presents a transparent, multi-metric trade-off characterization that integrates scale loss, metallic yield, specific fuel consumption, CO and NOx concentrations, and a process-boundary carbon-economic screening. This enables plant engineers and researchers to evaluate the recommended strategy against site-specific constraints.

2. Materials and Methods

2.1 Study Site and Furnace System

The study was conducted at a structural-steel hot-rolling mill in Thailand operating a natural-gas-fired walking-beam reheating furnace that has been in continuous production since 2010. The furnace has internal dimensions of approximately 24 m (length) × 13 m (width) × 5 m (height) and is organized into three primary combustion zones arranged along the direction of billet travel: a preheating zone (upstream, adjacent to the charging end), a heating zone (central), and a

soaking zone (downstream, adjacent to the discharge end). Walking-beam conveying enables continuous production without furnace emptying between campaigns. The system is equipped with low-NOx recuperative burners providing independent zone-level combustion control, and a Level II programmable control system manages zone temperatures, air-to-fuel ratios, and furnace pressure.

The discharge-end aperture (hereafter "door") constitutes the primary air-infiltration pathway. During normal production this door is periodically operated for maintenance access, temperature sampling, and product size change-overs. Its state—open or closed—was therefore treated as a controllable experimental factor with direct operational relevance. Figure 1 provides a schematic of the furnace identifying the three combustion zones, the walking-beam mechanism, the discharge door location and infiltration pathway, the flue-gas sampling point, and the pressure measurement and control location.

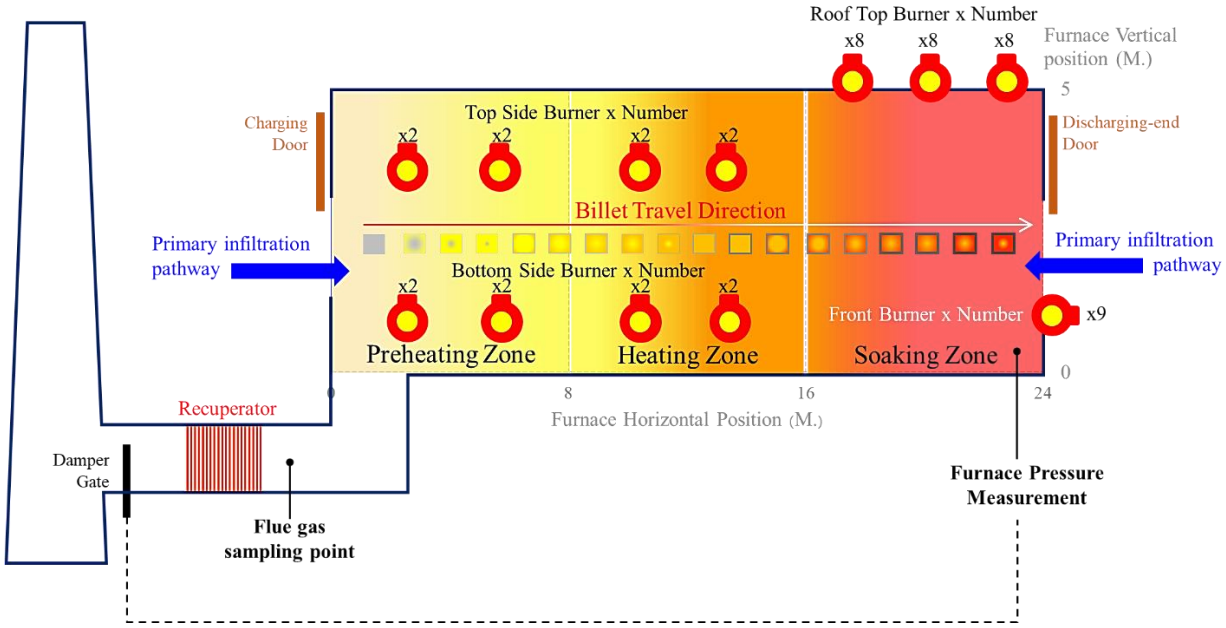

Figure 1 — Schematic of the industrial walking-beam reheating furnace. Annotations indicate the three combustion zones (preheating, heating, soaking), billet travel direction, discharge-end door (primary infiltration pathway), flue-gas sampling point (upstream of recuperator), and furnace pressure measurement location. Burner positions are represented by numbered arrows at each zone.

2.2 Instrumentation and Data Acquisition

Dry flue-gas O_2 was measured continuously by a stationary paramagnetic or zirconia-based electrochemical oxygben analyzer installed in the common flue duct upstream of the recuperator. All experimental readings were cross-validated with a calibrated portable electrochemical flue-gas analyzer (measurement uncertainty ±0.1% O_2 at 95% confidence, certified calibration traceable to national standards) inserted at the same duct location during each trial run. Steady-state criteria

required that dry flue-gas O_2, all three zone temperatures, and billet throughput had remained stable within prescribed tolerances for a minimum of 20 continuous minutes before any measurement was recorded, consistent with standard industrial combustion measurement practice.

CO and NOx were measured using a multi-gas instrumental analyzer following procedures consistent with U.S. EPA Reference Methods 10 (CO) and 7E (NOx), respectively, adapted for industrial process-heat applications. Calibration gas (certified traceable mixtures) and zero-gas checks were performed before and after each measurement sequence. Billet mass was recorded on certified platform scales (precision ±0.5 kg) at both the charge side (pre-furnace) and exit side (post-hydraulic descaling) for each replicate run. Natural-gas volumetric flow was measured by calibrated turbine meters on the supply header to each zone and corrected to standard conditions (0 °C, 101.325 kPa) to obtain Nm^3. Table 1 summarizes the instrumentation deployed.

Table 1. Summary of instrumentation used for data acquisition. All measurements were taken under stabilized steady-state conditions.

Parameter	Instrument Type	Accuracy / Uncertainty	Calibration / Standard
Dry flue-gas O_2 (%)	Stationary electrochemical analyzer + portable cross-check	±0.1% O_2 (95% CI)	Traceable to national standards; zero/span checked each run
CO and NOx (ppm)	Multi-gas instrumental analyzer	Per EPA Methods 10 & 7E	Certified calibration gas mixtures; pre/post-run checks
Billet mass (kg)	Certified platform scales	±0.5 kg	Legal-for-trade certification; in-use verification each shift
Natural-gas flow (Nm^3/h)	Calibrated turbine flow meters	±1.0% of reading	Factory calibration; corrected to 0 °C, 101.325 kPa
Furnace pressure (Pa)	Differential pressure transducer	±0.5 Pa	Manufacturer calibration; referenced to ambient

2.3 Experimental Design and Factor Levels

A replicated 2^3 full factorial design was employed to provide orthogonal, unconfounded estimates of all main effects and interaction effects among the three controllable factors (Montgomery, 2017). This design is particularly suited to industrial environments where experimental resources are limited and knowledge of the interaction structure—not just main effects—is essential for designing robust operating rules. The design comprised eight treatment combinations, each replicated independently in random run order, yielding 16 total observations. Run order was randomized to the fullest extent permitted by production scheduling to distribute nuisance

variation (ambient temperature, billet mix composition, operator shift) across treatments rather than confound it with specific factor levels.

The three factors and their two-level settings are defined in Table 2. Factor X1 (air–fuel strategy) contrasts conventional uniform excess-air control ($\lambda = 1.10$ in all three zones) against zone-differentiated lambda staging in which the soaking zone operates fuel-rich ($\lambda = 0.90$), the heating zone at stoichiometry ($\lambda = 1.00$), and the preheating zone with modest excess air ($\lambda = 1.10$). Factor X2 (furnace pressure) compares the lower (10 Pa) and upper (20 Pa) bounds of the plant's normal operating range. Factor X3 (door state) contrasts the discharge door fully closed versus a controlled door-open condition representative of a maintenance or inspection event.

Table 2. Factors, codes, and two-level settings in the replicated 2^3 full factorial experimental design. Total experimental runs: 16 (8 treatment combinations × 2 replicates).

Code	Factor	Low Level (−1)	High Level (+1)
X1	**Air–fuel control strategy (lambda, λ)**	Zone-differentiated lambda staging: soaking $\lambda = 0.90$; heating $\lambda = 1.00$; preheating $\lambda = 1.10$	Uniform excess air: $\lambda = 1.10$ in all three combustion zones
X2	**Furnace pressure setpoint (Pa)**	10 Pa	20 Pa
X3	**Discharge-door state**	Closed (sealed)	Open (controlled event)

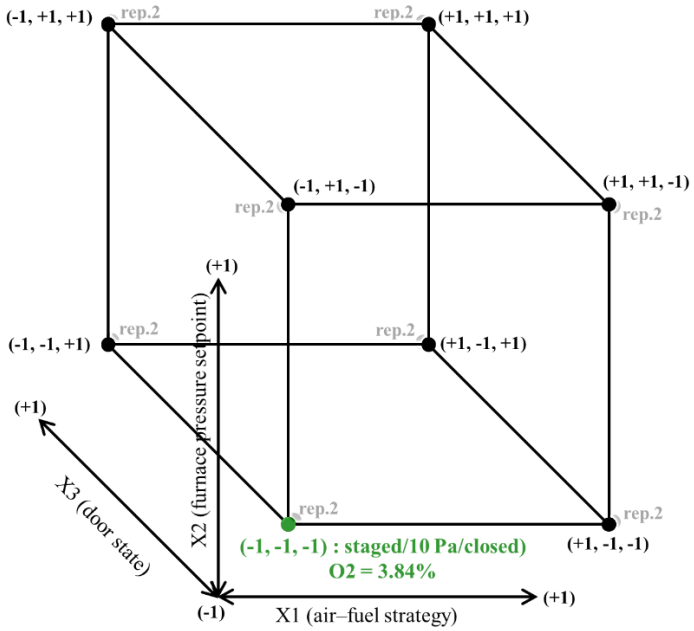

Figure 2 — Geometric representation of the 2^3 factorial design space. Each of the eight vertices represents one treatment combination defined by X1 (air–fuel strategy), X2 (furnace pressure setpoint), and X3 (door state) at their coded low (−1) and high (+1) levels. Two independent

replicates were conducted at each vertex. The highlighted vertex (X1 = −1, X2 = −1, X3 = −1: staged/10 Pa/closed) corresponds to the treatment that yielded the minimum observed O_2 = 3.84%.

2.4 Response Variables and Derived Quantities

The primary response was dry flue-gas O_2 concentration (Y1, %). Secondary responses were: (Y2) specific oxidation scale loss (kg/t steel) and metallic yield (%); (Y3) specific natural-gas consumption (Nm^3/t steel); and (Y4–Y5) CO and NOx concentrations in the flue gas (ppm, dry basis). Scale loss and yield were derived from paired billet mass measurements:

$$\text{Scale loss (kg/t)} = 1000 \times (m_{in} - m_{out}) / m_{in} \quad \textit{(Eq. 1)}$$

$$\text{Yield (\%)} = 100 \times m_{out} / m_{in} \quad \textit{(Eq. 2)}$$

where m_{in} is the charged billet mass (kg) and m_{out} is the mass after hydraulic descaling (kg). Where emission concentrations are compared across conditions with different flue-gas O_2 levels, a dry oxygen correction to a 3% O_2 reference basis was applied:

$$C_{ref} = C_{meas} \times (21 - O_{2,ref}) / (21 - O_{2,meas}) \quad \textit{(Eq. 3)}$$

where C_{ref} is the corrected concentration at the 3% O_2 reference, C_{meas} is the measured concentration, and $O_{2,meas}$ is the measured dry flue-gas O_2 (%). Both corrected and as-measured values are reported for transparency.

2.5 Statistical Analysis

The 16-observation factorial dataset was analyzed by ordinary least squares (OLS) regression under coded factor levels (−1, +1), ensuring orthogonality of effect estimates and equal variance across the factorial space. The fitted model included all three main effects, all three two-factor interactions, and the three-factor interaction—seven terms in total (Montgomery, 2017). Under coded parameterization, each regression coefficient equals one-half of the corresponding factorial effect (defined as the high-minus-low difference, averaged over all combinations of the remaining factors). Model adequacy was assessed through R^2 and adjusted R^2, and residual diagnostics including normal probability plots and plots of residuals versus fitted values, run order, and individual factor levels. All effect estimates are reported with 95% confidence intervals and two-sided p-values from t-tests at $\alpha = 0.05$.

2.6 Carbon-Economic Screening

A process-boundary carbon-economic screening translated operational changes into carbon-equivalent and monetary terms. The screening boundary encompasses only the direct combustion process: it credits avoided embodied emissions from reduced scale loss and debits added combustion emissions from increased fuel use, but excludes upstream fuel-cycle emissions, downstream steel processing, and system-level life-cycle effects.

The avoided embodied burden from scale loss reduction was estimated at 2.00 kg CO_2e/kg steel (screening proxy for cradle-to-gate carbon intensity of structural steel). The combustion emissions penalty was estimated at 1.90 kg CO_2e/Nm^3 natural gas (IPCC Tier 1 lower-heating-value stationary combustion). The net process-boundary carbon change is:

$$\Delta C\_net\ (kg\ CO_2e/t) = -(\Delta scale \times 2.00) + (\Delta NG \times 1.90) \quad \textit{(Eq. 4)}$$

where Δscale is the reduction in scale loss (kg/t, positive when reduced) and ΔNG is the increase in natural-gas consumption (Nm^3/t, positive when increased). Economic parameters are summarized in Table 3.

Table 3. Economic and carbon-conversion parameters used in the process-boundary carbon-economic screening analysis

Value	Basis and Purpose in Screening
588 USD/t	Revenue value of recovered metallic yield
0.12 USD/kg scale	Operational saving from reduced oxidation waste
0.28 USD/Nm^3	Fuel-cost penalty under staged low-O_2 control
2.00 kg CO_2e/kg steel	Screening proxy for cradle-to-gate carbon intensity (avoided upstream production)
1.90 kg CO_2e/Nm^3	IPCC Tier 1 lower-heating-value stationary combustion assumption
70 USD/tCO_2e	Consistent with World Bank (2025) high-scenario carbon pricing coverage

3. Results and Discussion

3.1 Excess-Oxygen Response Across the Full Factorial Space

Across 16 experimental runs, dry flue-gas O_2 ranged from 3.84% to 13.17% (grand mean = 7.23%; SD = 2.90%), confirming that excess oxygen in industrial walking-beam reheating is not a narrow stoichiometric trimming problem but a disturbance-sensitive system in which combustion management and infiltration-boundary conditions interact strongly. The full range of 9.33 %-points—nearly three times the grand mean minus the minimum—demonstrates the magnitude of control leverage available to operators. Observed treatment means and within-cell standard deviations are reported in Table 4. The consistency of within-cell SDs (0.085–1.117 %-points), small relative to inter-treatment differences, confirms that process conditions were sufficiently stable within runs and that replicate error was small relative to treatment effects, supporting statistical power for the subsequent factorial analysis.

Run Conditions	X1: Air–Fuel Strategy	X2: Pressure (Pa)	X3: Door State	Mean O_2 (%)	SD (%)
Best	Staged (λ staging)	10	Closed	3.900	0.085
	Staged (λ staging)	10	Open	6.535	0.346
	Staged (λ staging)	20	Closed	4.270	0.198
	Staged (λ staging)	20	Open	5.155	0.276
Ref.	Uniform (λ = 1.10)	10	Closed	7.040	0.156
Worst	Uniform (λ = 1.10)	10	Open	12.825	0.488
	Uniform (λ = 1.10)	20	Closed	8.095	0.177
	Uniform (λ = 1.10)	20	Open	10.020	1.117

Table 4. Observed mean dry flue-gas O_2 (%) and within-cell standard deviation (n = 2 per cell). "Best" = minimum O_2 (optimal); "Ref." = baseline conventional practice (uniform/10 Pa/closed); "Worst" = maximum O_2. Green = favorable; red = unfavorable.

Three patterns are immediately evident. First, lambda staging consistently produced substantially lower O_2 than the uniform strategy across every combination of pressure and door state, confirming the primacy of stoichiometric management. Second, door-open conditions elevated O_2 by 1.3–5.8 %-points depending on pressure, confirming the important—and variable—role of infiltration. Third, the effect of pressure was directionally reversed between the door-closed and door-open conditions: under door-closed, higher pressure slightly increased O_2 (from 3.90% to 4.27% and from 7.04% to 8.10% under staged and uniform, respectively), whereas under door-open, higher pressure reduced O_2 (from 6.54% to 5.16% and from 12.83% to 10.02%). This directional reversal is the empirical signature of the pressure × door interaction and is the mechanistic foundation of the conditional control rule developed in Section 3.2.

3.2 Factorial Effect Estimates, Model Fit, and Statistical Inference

The replicated 2^3 model (Eq. 5) achieved $R^2 = 0.986$ and adjusted $R^2 = 0.974$, accounting for 98.6% of total O_2 variation with seven factorial terms. Residual diagnostics revealed no systematic departures from normality or homoscedasticity. The fitted model in coded factor units is:

$$\hat{Y}_1 = 7.230 + 2.265X_1 - 0.345X_2 + 1.404X_3 - 0.093X_1X_2 + 0.524X_1X_3 - 0.701X_2X_3 - 0.264X_1X_2X_3 \quad \textit{(Eq. 5)}$$

Factorial effect estimates (high minus low, averaged over all combinations of the remaining factors) are reported in Table 5 with 95% confidence intervals and p-values.

Term	Description	Effect Estimate (ΔO_2, %-points)	95% Confidence Interval	p-value
X_1	**Air–fuel strategy (uniform vs. staged)**	**+4.53**	[+3.99, +5.07]	**< 0.001**
X_2	Furnace pressure (20 Pa vs. 10 Pa)	−0.69	[−1.23, −0.15]	0.019
X_3	**Door state (open vs. closed)**	**+2.81**	[+2.26, +3.35]	**< 0.001**
$X_1 \times X_2$	Air–fuel × pressure interaction	−0.18	[−0.73, +0.36]	0.456
$X_1 \times X_3$	**Air–fuel × door interaction**	**+1.05**	[+0.50, +1.59]	**0.002**
$X_2 \times X_3$	**Pressure × door interaction**	**−1.40**	[−1.95, −0.86]	**< 0.001**
$X_1 \times X_2 \times X_3$	Three-factor interaction	−0.53	[−1.07, +0.02]	0.056

Table 5. Factorial effect estimates for dry flue-gas O_2 from the replicated 2^3 model ($R^2 = 0.986$; adj. $R^2 = 0.974$). Bold rows indicate statistically significant effects ($\alpha = 0.05$). Effect = high-level minus low-level difference averaged over all combinations of remaining factors.

The dominant main effect is the air–fuel strategy: switching from staged to uniform excess air increases mean O_2 by +4.53 %-points (95% CI: [3.99, 5.07]; $p < 0.001$). This is physically explained by the elimination of the sub-stoichiometric soaking zone ($\lambda = 0.90$) under the uniform strategy, which removes an oxygen-consumption mechanism active under staging. The door-state main effect is also large and highly significant (+2.81 %-points; $p < 0.001$), reflecting the substantial infiltration load introduced during door-open events. The furnace pressure main effect is statistically significant but smaller (−0.69 %-points; $p = 0.019$), confirming that pressure alone provides limited oxygen control.

The most important interaction is $X_2 \times X_3$ (pressure × door state): −1.40 %-points ($p < 0.001$). The negative sign indicates that the effect of increasing pressure from 10 to 20 Pa is substantially more oxygen-reducing (beneficial) when the door is open than when it is closed—consistent with infiltration physics, in which a greater positive pressure differential more effectively resists inward ambient-air flow through an open aperture (Trinks et al., 2004). The $X_1 \times X_3$ interaction is also significant (+1.05 %-points; $p = 0.002$): the O_2 penalty of door opening is larger under uniform excess-air operation than under staged control. The three-factor interaction is borderline ($p = 0.056$); the $X_1 \times X_2$ interaction is not significant ($p = 0.456$).

The interaction plot (Figure 3) visualizes the $X_2 \times X_3$ interaction stratified by air–fuel strategy. The crossing or near-crossing of lines between the door-closed and door-open conditions at each pressure level is the graphical confirmation of the interaction and directly motivates the conditional control rule.

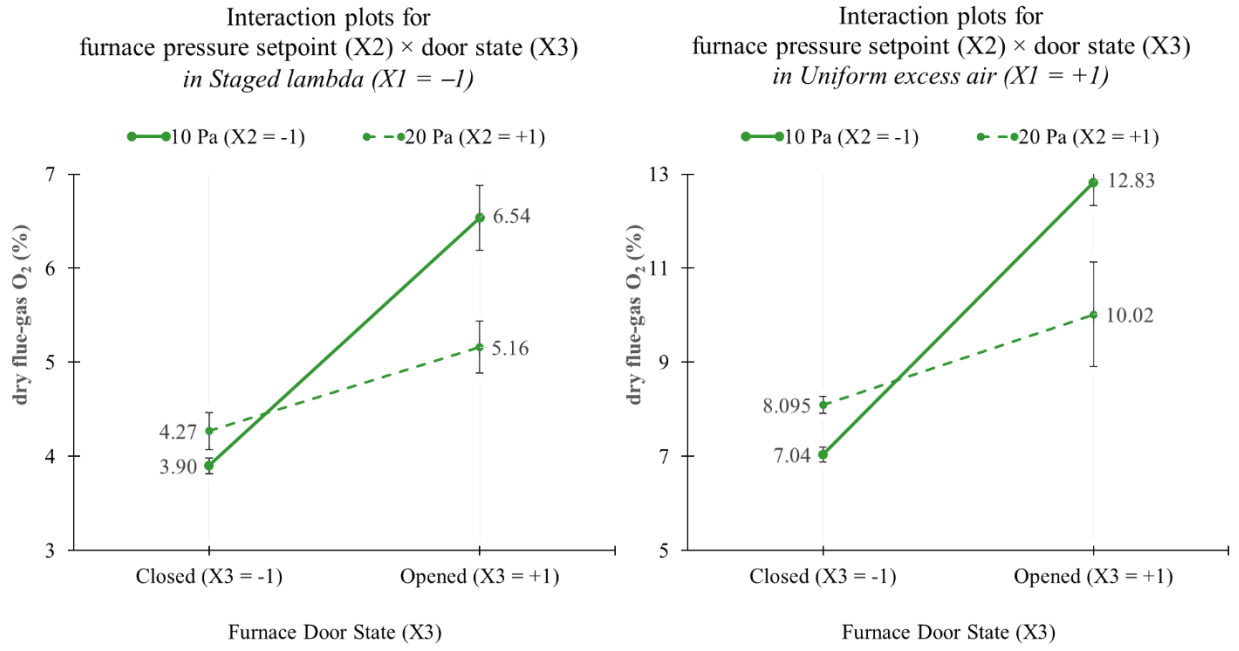

Figure 3 — Interaction plots for furnace pressure setpoint (X2) × door state (X3), separately for each air–fuel strategy (left panel: staged lambda; right panel: uniform excess air). The y-axis represents mean dry flue-gas O_2 (%). Solid lines connect door-closed observations; dashed lines connect door-open observations. The reversal in the direction of the pressure effect between door-closed and door-open conditions (line crossing) confirms the statistically significant $X_2 \times X_3$ interaction (−1.40 %-points, $p < 0.001$). Error bars represent ±1 within-cell standard deviation.

3.2.1 Conditional Oxygen-Control Rule

The factorial interaction structure directly yields a practical, door-state-conditional control rule implementable in existing Level II systems:

- Door CLOSED → Staged lambda (X1 = −1) + Pressure = 10 Pa (X2 = −1): Predicted mean O_2 ≈ 3.90%. Rationale: infiltration pathway is sealed; higher pressure provides no additional benefit and slightly increases O_2 (possibly through increased short-circuit flue-gas flow); staged combustion achieves minimum stoichiometric O_2.
- Door OPEN → Staged lambda (X1 = −1) + Pressure = 20 Pa (X2 = +1): Predicted mean O_2 ≈ 5.16% vs. 6.54% at 10 Pa. Rationale: increased positive pressure differential suppresses infiltration-driven O_2 excursion by approximately 1.38 %-points during door events, limiting scale-loss penalty.

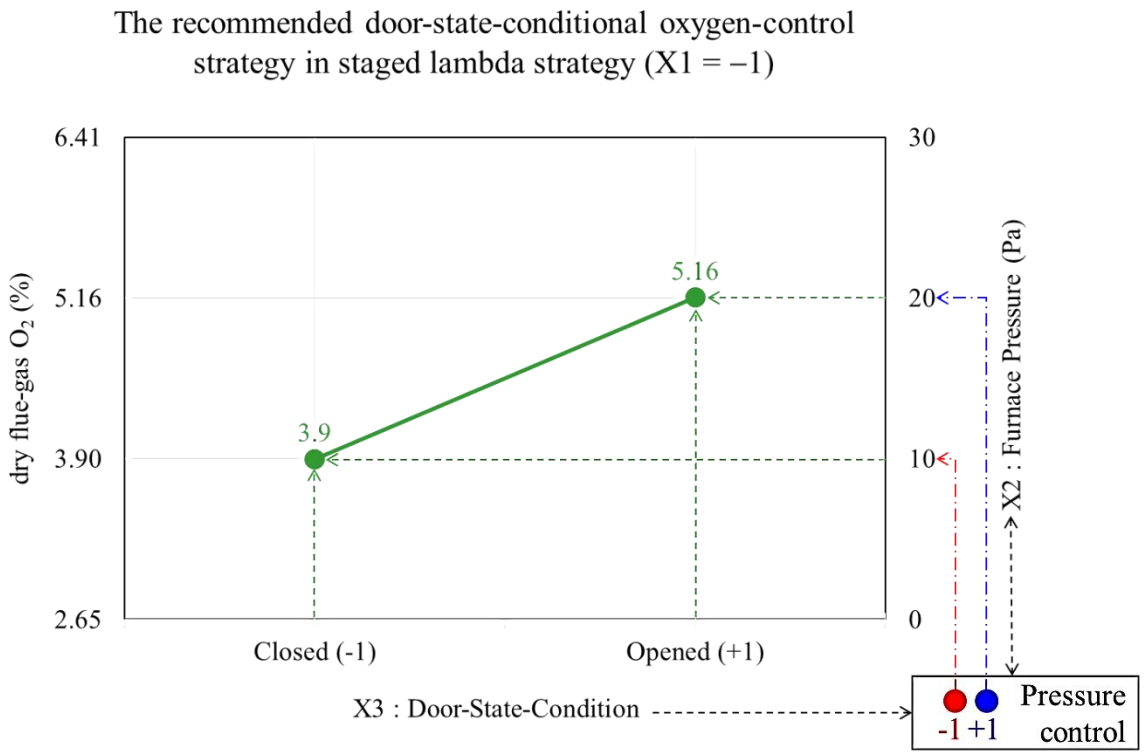

Figure 4 — Schematic of the recommended door-state-conditional oxygen-control strategy. When the door is closed, staged lambda control at 10 Pa is applied (O_2 target ≈ 3.90%). When the door opens, pressure is automatically increased to 20 Pa to suppress air infiltration while staged lambda control is maintained (O_2 target ≈ 5.16%). The door-position signal triggers the pressure setpoint switch in the Level II combustion-control system. Estimated O_2 excursion without pressure adjustment shown as dashed line for comparison.

3.3 Secondary Performance Responses: Scale, Yield, Fuel, and Emissions

Table 6 presents the comprehensive performance comparison between the baseline conventional regime (uniform excess air, 10 Pa, door closed—the current plant practice) and the

recommended door-state-conditional regime. Each metric is discussed in subsections below. Table 6. Comprehensive performance comparison: baseline conventional regime vs. recommended door-state-conditional oxygen-control strategy. pp = percentage points; ref. = reference (zero by definition). Green = improvement; red = penalty.

Performance Metric	Baseline Regime	Recommended Regime	Absolute Change	Interpretation
Atmosphere & Oxidation				
Dry flue-gas O_2 (%)	7.04	3.90	−3.14 (−44.6%)	Substantially lower oxidation driving force
Scale loss (kg/t steel)	21.64	17.82	−3.82 (−17.7%)	Major reduction in surface oxidation waste
Metallic yield (%)	97.83	98.21	+0.38 pp	Higher saleable output per tonne charged
Energy				
Specific natural gas consumption (Nm^3/t)	48.29	53.81	+5.52 (+11.4%)	Fuel penalty from staged combustion and lower recuperator preheat
Emissions				
CO (ppm, dry, uncorrected)	< 1	22	+22	Increased incomplete-combustion risk at lower O_2
NOx (ppm, dry, uncorrected)	12	14	+2	Marginal increase; remained well within limits
Carbon & Economics				
Net carbon change (kg CO_2e/t steel)	0.00 (ref.)	+2.85	+2.85	Small process-boundary increase; partially offset by material efficiency
Net economic value (USD/t steel)	0.00 (ref.)	+0.94	+0.94	Positive net operating gain after fuel penalty and carbon cost

3.3.1 Scale Loss and Metallic Yield

The 17.7% reduction in specific scale loss (−3.82 kg/t steel) is the primary material-efficiency benefit of the recommended regime. This magnitude is consistent with oxidation-kinetic theory: scale growth rate follows a parabolic law with O_2 partial pressure as the primary driving variable at the steel surface (Kofstad, 1988), so a reduction from 7.04% to 3.90% O_2 in the furnace atmosphere substantially lowers the effective oxidation rate, particularly in the soaking zone where residence time is longest. Recent industrial-scale and semi-industrial experiments confirm that atmosphere composition, including O_2 content and the partial pressures of CO_2 and H_2O, significantly modulates scale layer growth rate, morphology, and adherence (Schwarz et al., 2025; Xu et al., 2024). At a representative throughput of 100 t/h, the 3.82 kg/t improvement represents 382 kg/h of additional saleable steel—approximately 3,300 t/year for a furnace operating 8,700 h/year—with direct revenue implications.

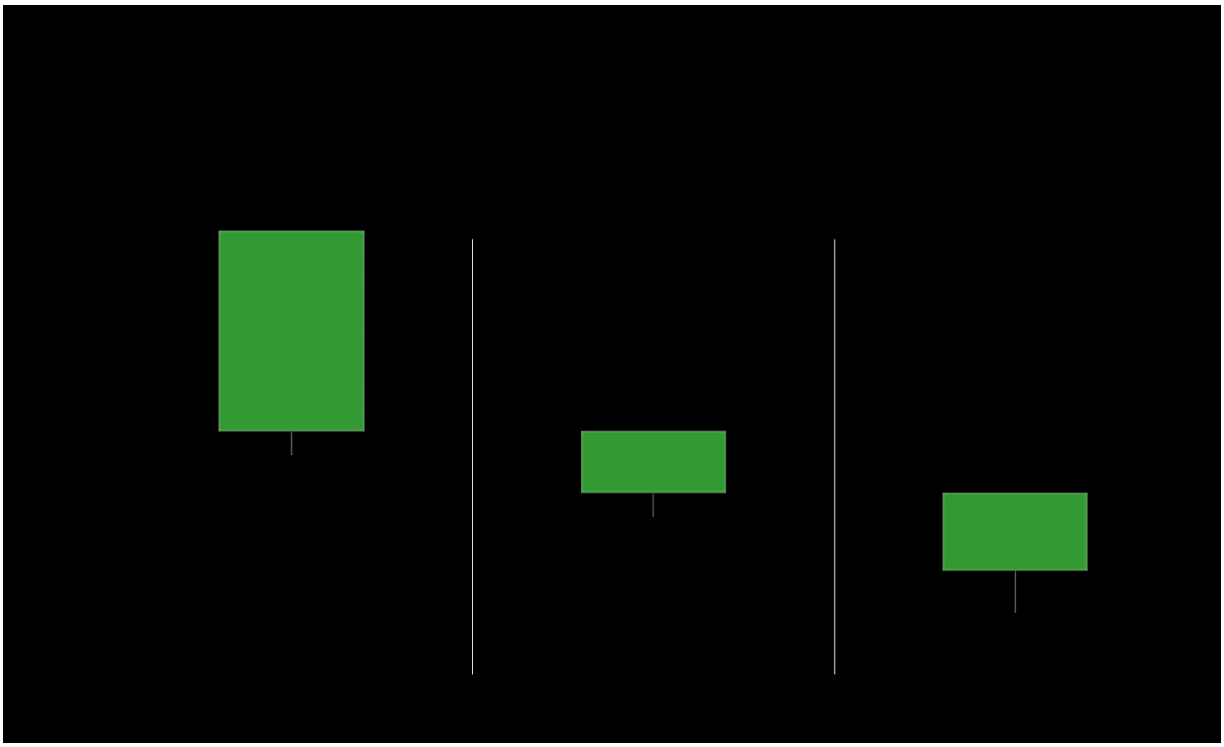

Figure 5 — Waterfall chart: Decomposition of the scale-loss reduction (−3.82 kg/t steel) into contributions from: (a) air–fuel strategy change (X1 main effect), (b) pressure setpoint effect during door-open events (X2 × X3 interaction benefit), and (c) residual interaction terms. Values are derived from the factorial model (Eq. 5) evaluated at the recommended vs. baseline factor settings. Error bars represent 95% confidence intervals of the modeled contribution.

3.3.2 Specific Fuel Consumption

Specific natural-gas consumption increased from 48.29 to 53.81 Nm^3/t (+11.4%; +5.52 Nm^3/t). This fuel penalty arises from two mechanisms. First, operating the soaking zone at $\lambda = 0.90$ (sub-stoichiometric) under lambda staging redistributes heat release, producing a longer, more luminous flame that alters the local radiative heat-transfer field and may require additional fuel to achieve

the target discharge temperature. Second, lower excess O_2 reduces the sensible heat content of the flue gas recovered by the recuperator, thereby increasing net fuel demand for a given air preheat temperature. These mechanisms are directionally consistent with computational and experimental findings from recent reheating-furnace optimization studies (Khalid et al., 2021; Lu et al., 2025; Zhao et al., 2025). The fuel penalty is a genuine trade-off and must be weighed against material-efficiency gains in the economic screening (Section 3.4).

3.3.3 Combustion Emissions: CO and NOx

CO increased from < 1 ppm to 22 ppm under the recommended low-O_2 regime. This is consistent with the fundamental combustion chemistry of near-stoichiometric and sub-stoichiometric conditions: as λ approaches or falls below 1.0 in the soaking zone, the probability of incomplete oxidation of CO to CO_2 increases owing to reduced available O_2 and lower local flame temperatures. While 22 ppm CO represents an increase in incomplete-combustion risk, it remains substantially below typical regulatory thresholds for large industrial combustion plants (generally 100–250 mg/Nm³, or approximately 90–225 ppm at 3% O_2 reference, in most jurisdictions). NOx showed only a marginal increase of 2 ppm (12 → 14 ppm), remaining within a very narrow absolute range. This behavior is consistent with the theoretical and experimental basis of staged combustion for thermal-NOx suppression: by reducing peak flame temperatures and localized O_2 availability in the stoichiometry-sensitive soaking zone, staged-air control suppresses thermal-NO formation even as CO risk modestly increases—a well-documented trade-off in low-NOx reheating-furnace design (Sung et al., 2021).

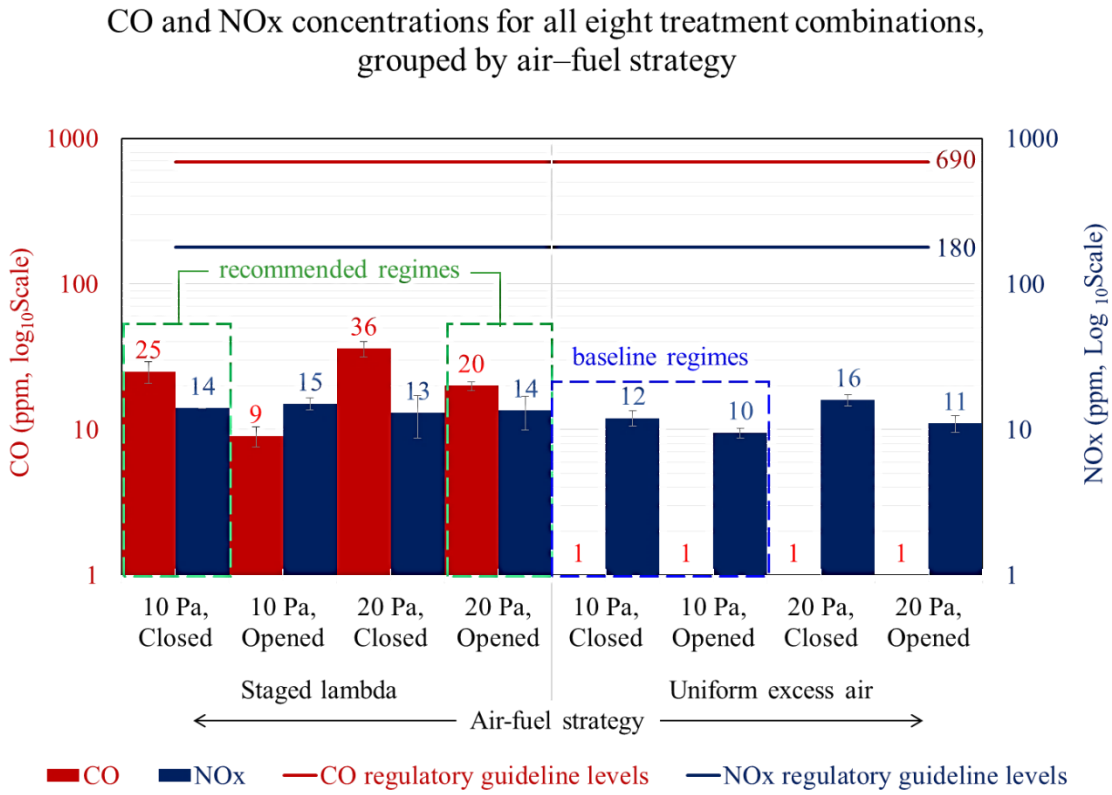

Figure 6 — Dual-axis bar chart showing CO (left y-axis, ppm) and NOx (right y-axis, ppm) concentrations for all eight treatment combinations, grouped by air–fuel strategy. Baseline and recommended regimes are highlighted. Dashed reference lines indicate illustrative regulatory guideline levels for context. Error bars represent within-cell standard deviation. The trade-off between CO (increasing under lower-O_2 conditions) and NOx (stable-to-slightly-reduced) is clearly visible.

3.4 Carbon-Economic Trade-off Analysis

Applying Equation 4 with the parameters in Table 3: the scale-loss reduction of 3.82 kg/t steel avoids 7.64 kg CO_2e/t (= 3.82 × 2.00), while the natural-gas increase of 5.52 Nm^3/t adds 10.49 kg CO_2e/t (= 5.52 × 1.90). The net process-boundary carbon change is therefore +2.85 kg CO_2e/t steel. Under the 70 USD/tCO_2e scenario, this corresponds to a carbon cost of 0.20 USD/t steel.

The combined operational benefit—yield recovery revenue from 3.82 kg additional steel at 588 USD/t (≈ 2.25 USD/t) plus scale-handling cost saving from 3.82 kg/t at 0.12 USD/kg (≈ 0.46 USD/t) totalling approximately 2.71 USD/t—minus the fuel-cost penalty (5.52 Nm^3/t × 0.28 USD/Nm^3 = 1.55 USD/t) and carbon cost (0.20 USD/t) yields a net economic gain of approximately +0.96 USD/t steel (approximately +0.94 USD/t after rounding in the original screening). This positive net value is robust under sensitivity analysis: the net benefit remains

positive even if the natural-gas price doubles or the billet price falls by 15%, reflecting the strong leverage of even modest yield improvements at steel market prices.

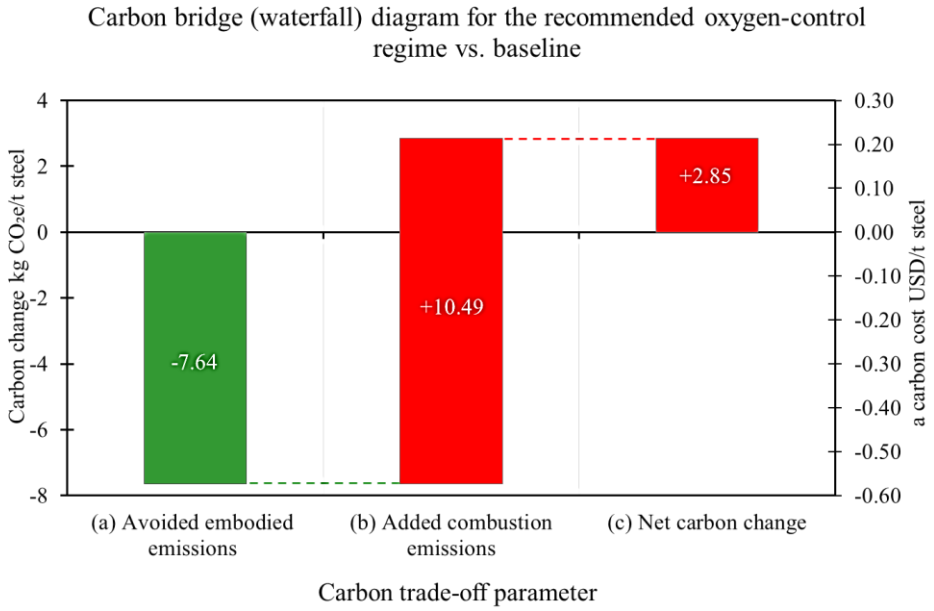

Figure 7 — Carbon bridge (waterfall) diagram for the recommended oxygen-control regime vs. baseline. Left-to-right bars: (1) Avoided embodied emissions from scale-loss reduction: −7.64 kg CO_2e/t steel (benefit, green); (2) Added combustion emissions from fuel increase: +10.49 kg CO_2e/t steel (penalty, red); (3) Net process-boundary carbon change: +2.85 kg CO_2e/t steel (small net increase, amber). A secondary axis (right) shows the economic equivalents in USD/t steel at 70 USD/tCO_2e.

It is important to contextualize this result: the +2.85 kg CO_2e/t is a process-boundary screening value, not a full life-cycle assessment. It reflects the near-term combustion reality of existing fuel-fired assets and should be interpreted as an efficiency-first measure that improves material output and economic performance while the sector pursues longer-term deep-decarbonization pathways—consistent with the analytical framing advocated in recent industrial decarbonization literature (IEA, 2023; Kim et al., 2024; McMillan & Wachs, 2024).

3.5 Industrial Implications and Study Limitations

3.5.1 Practical Implications

The central operational insight of this study is not simply that lower oxygen is better, but that effective oxygen control requires a conditional, multi-input strategy that accounts explicitly for the infiltration dynamics associated with door events. The recommended rule—switch pressure setpoint from 10 to 20 Pa in response to door-open events, while maintaining lambda staging—is implementable in existing Level II control systems via a door-position signal without hardware modification or capital expenditure. This type of event-triggered adaptive control represents a

straightforward but overlooked refinement of current practice in many industrial reheating facilities.

3.5.2 Limitations and Scope Boundaries

The study should be interpreted within four clearly stated scope boundaries. First, it is a single-plant case study; quantitative results (optimal pressure setpoints, magnitude of fuel penalty, CO/NOx balance) may differ in furnaces with different burner arrangements, door geometry, throughput profiles, or fuel specifications. Validation in additional furnaces is warranted before generalizing specific numerical recommendations. Second, the carbon-economic analysis is a process-boundary screening, not a full life-cycle assessment; emission factors are generic screening values rather than plant-measured quantities. Third, CO and NOx are reported in concentration terms; regulatory compliance assessment requires mass-based normalization (mg/Nm^3) with jurisdiction-specific reference-O_2 correction. Fourth, the experimental period covers the 16 planned factorial runs; longer validation campaigns across full production seasons, billet grade mixes, and ambient conditions would strengthen generalizability. Future work should additionally investigate the frequency distribution of door-open events in continuous rolling campaigns and quantify the cumulative O_2 excursion load attributable to infiltration over extended production periods.

4. Conclusion

This full-scale industrial 2^3 factorial study established that excess-oxygen optimization in a natural-gas-fired walking-beam reheating furnace is a coupled stoichiometry–infiltration problem that requires a conditional, adaptive control strategy—not a simple excess-air trimming adjustment. The key findings are summarized as Air–fuel strategy is the dominant oxygen-control lever: switching from uniform excess air ($\lambda = 1.10$ in all zones) to zone-differentiated lambda staging (soaking $\lambda = 0.90$; heating $\lambda = 1.00$; preheating $\lambda = 1.10$) reduced mean dry flue-gas O_2 by +4.53 %-points ($p < 0.001$), independent of pressure or door state. Door state is the second most important factor (+2.81 %-points, $p < 0.001$), confirming that discharge-door infiltration is a major and under-controlled O_2 source in industrial walking-beam furnaces. The furnace pressure × door-state interaction (−1.40 %-points, $p < 0.001$) is the critical mechanistic finding: higher pressure suppresses infiltration-driven O_2 excursions when the door is open, but provides limited or slightly adverse benefit when the door is closed. This interaction necessitates a conditional control rule. The recommended door-state-conditional strategy (staged lambda + 10 Pa/closed; staged lambda + 20 Pa/open) reduced mean O_2 from 7.04% to 3.90%, lowered scale loss by 17.7% (21.64 → 17.82 kg/t steel), and raised metallic yield from 97.83% to 98.21%—with a net economic gain of approximately +0.94 USD/t steel after accounting for an 11.4% increase in specific fuel consumption and a small CO increase to 22 ppm. The process-boundary carbon trade-off is small (+2.85 kg CO_2e/t steel) and economically manageable (+0.20 USD/t at 70 USD/tCO_2e), positioning this strategy as an efficiency-first operational measure compatible with longer-term

decarbonization transitions. This study provides a statistically grounded, physically interpretable, and directly implementable framework for excess-oxygen management in existing fuel-based reheating furnaces, with explicit quantification of the energy, emissions, and economic trade-offs that industrial decision-makers require. The conditional control rule derived from the factorial interaction structure can be deployed without capital investment and is compatible with existing Level II combustion-control architectures.

Practical Recommendations for Implementation

Deploy door-state-conditional pressure control: integrate the door-position signal into the Level II system to automatically switch the furnace pressure setpoint between 10 Pa (door closed) and 20 Pa (door open). Implement zone-differentiated lambda staging: configure soaking $\lambda = 0.90$, heating $\lambda = 1.00$, and preheating $\lambda = 1.10$ with regular burner-calibration checks to maintain zone-level accuracy. Monitor CO continuously as the primary online indicator of combustion completeness under low-O_2 staged conditions; set a CO alarm threshold below applicable regulatory limits.Conduct a long-term validation campaign (minimum one full rolling season, ≥ 3 months) to quantify performance across the full range of billet grades, throughput levels, and ambient conditions at the specific site. For sites with high door-event frequency, quantify the cumulative infiltration O_2 load over a production campaign to assess whether additional sealing improvements or door-management protocols provide complementary benefits.

Declarations

Conflict of Interest Statement

The authors declare no known competing financial interests or personal relationships that could have appeared to influence the work reported in this manuscript.

Data Availability Statement

The plant operating data used in this case study are commercially sensitive and subject to a confidentiality agreement with the host facility. Aggregated summary data supporting the main findings are reported in full in the manuscript tables. Additional anonymized data may be made available by the corresponding author upon reasonable request, subject to written approval by plant management.

Funding

This research received no specific grant from any funding agency in the public, commercial, or not-for-profit sectors.

Author Contributions

Peerakarn Banjerdkij: Conceptualization, Methodology, Investigation, Formal Analysis, Writing – Original Draft, Writing – Review & Editing. Gan Yimyam: Investigation, Data Curation, Validation, Writing – Review & Editing.

References

Gan, Z., Yang, S., & Wang, H. (2024). Investigation of the heating characteristics of turbulent non-premixed gas combustion in the industrial-scale walking beam type reheating furnace. Applied Thermal Engineering, 257(Part B), Article 124212. https://doi.org/10.1016/j.applthermaleng.2024.124212

International Energy Agency. (2023). Iron and steel technology roadmap: Towards more sustainable steelmaking. IEA Publications. https://www.iea.org/reports/iron-and-steel-technology-roadmap

Khalid, Y., Wu, M., Silaen, A., Martinez, F., Okosun, T., Worl, B., Low, J., Zhou, C., Johnson, K., & White, D. (2021). Oxygen enrichment combustion to reduce fossil energy consumption and emissions in hot rolling steel production. Journal of Cleaner Production, 320, Article 128714. https://doi.org/10.1016/j.jclepro.2021.128714

Kim, J., Sovacool, B. K., Bazilian, M., Griffiths, S., Lee, J., Yang, M., & Lee, J. (2022). Decarbonizing the iron and steel industry: A systematic review of sociotechnical systems, technological innovations, and policy options. Energy Research & Social Science, 89, Article 102565. https://doi.org/10.1016/j.erss.2022.102565

Kim, J., Sovacool, B. K., Bazilian, M., Griffiths, S., & Yang, M. (2024). Energy, material, and resource efficiency for industrial decarbonization: A systematic review of sociotechnical systems, technological innovations, and policy options. Energy Research & Social Science, 112, Article 103521. https://doi.org/10.1016/j.erss.2024.103521

Kofstad, P. (1988). High temperature corrosion. Elsevier Applied Science.

Lu, B., Wang, X., Chen, D., Wang, H., Hu, Q., Chen, Y., & Huang, M. (2025). Energy saving study of reheating furnace from structure and oxygen-enriched combustion. Applied Thermal Engineering, 263, Article 125337. https://doi.org/10.1016/j.applthermaleng.2024.125337

McMillan, C. A., & Wachs, L. (2024). Industrial process heat decarbonization: A user-centric perspective. Energy Research & Social Science, 112, Article 103505. https://doi.org/10.1016/j.erss.2024.103505

Montgomery, D. C. (2017). Design and analysis of experiments (9th ed.). Wiley.

Schwarz, S., Daurer, G., Plank, B., Krull, H.-G., Szittnick, A., Lakhdari, M. A., Collin, S., Gasca, P., Chauveau, E., Deville-Cavellin, C., Demuth, M., Gaber, C., & Hochenauer, C. (2025). A comparative experimental analysis of the scale formation of various steel grades during reheating under hydrogen and natural gas air–fuel and oxy-fuel combustion conditions. International Journal of Hydrogen Energy, 101, 1105–1115. https://doi.org/10.1016/j.ijhydene.2024.12.279

Sung, Y., Kim, S., Jang, B., Oh, C., Jee, T., Park, S., Park, K., & Chang, S. (2021). Nitric oxide emission reduction in reheating furnaces through burner and furnace air-staged combustions. Energies, 14(6), Article 1599. https://doi.org/10.3390/en14061599

Trinks, W., Mawhinney, M. H., Shannon, R. A., Reed, R. J., & Garvey, J. R. (2004). Industrial furnaces (6th ed.). Wiley-Interscience.

World Bank. (2025). State and trends of carbon pricing 2025. World Bank Group. https://www.worldbank.org/en/publication/state-and-trends-of-carbon-pricing

World Steel Association. (2025). Sustainability indicators report 2025. https://worldsteel.org/wider-sustainability/sustainability-indicators/sustainability-indicators-report-2025/

Xu, J., Li, B., & Qi, F. (2024). Oxidation model of slabs in an industrial-scale walking-beam reheating furnace with mixed loading. Applied Thermal Engineering, 256, Article 124119. https://doi.org/10.1016/j.applthermaleng.2024.124119

Zhao, M., Li, X., & Hu, X. (2025). Study on flow and heat transfer characteristics of reheating furnaces under oxygen-enriched conditions. Processes, 13(8), Article 2454. https://doi.org/10.3390/pr13082454